Convective Modes for Significant Severe Thunderstorms in the Contiguous United States. Part II: Supercell and QLCS Tornado Environments

RICHARD L. THOMPSON, BRYAN T. SMITH, JEREMY S. GRAMS, ANDREW R. DEAN, AND CHRIS BROYLES

NOAA/NWS/NCEP/Storm Prediction Center, Norman, Oklahoma

(Manuscript received 4 October 2011, in final form 7 April 2012)

ABSTRACT

A sample of 22 901 tornado and significant severe thunderstorm events, filtered on an hourly 40-km grid, was collected for the period 2003–11 across the contiguous United States (CONUS). Convective mode was assigned to each case via manual examination of full volumetric radar data (Part I of this study), and environmental information accompanied each grid-hour event from the hourly objective analyses calculated and archived at the Storm Prediction Center (SPC). Sounding-derived parameters related to supercells and tornadoes formed the basis of this investigation owing to the dominance of right-moving supercells in tornado production and the availability of supercell-related convective parameters in the SPC environmental archive. The tornado and significant severe thunderstorm events were stratified by convective mode and season. Measures of buoyancy discriminated most strongly between supercell and quasi-linear convective system (QLCS) tornado events during the winter, while bulk wind differences and storm-relative helicity were similar for both supercell and QLCS tornado environments within in each season. The larger values of the effective-layer supercell composite parameter (SCP) and the effective-layer significant tornado parameter (STP) favored right-moving supercells that produced significant tornadoes, as opposed to weak tornadoes or supercells that produced only significant hail or damaging winds. Additionally, mesocyclone strength tended to increase with increasing SCP for supercells, and STP tended to increase as tornado damage class ratings increased. The findings underscore the importance of convective mode (discrete or cluster supercells), mesocyclone strength, and near-storm environment (as represented by large values of STP) in consistent, real-time identification of intense tornadoes.

1. Introduction

Proximity soundings have a long history of use in identifying the characteristics of severe storm environments, dating back to the 1940s (Showalter and Fulks 1943) and 1950s (e.g., Fawbush and Miller 1954; Beebe 1955, 1958). This early work has continued into the past two decades when additional proximity sounding samples were constructed by Johns et al. (1993), Rasmussen and Blanchard (1998, hereafter RB98), Rasmussen (2003), and Craven and Brooks (2004). These studies either relied on implicit assumptions (e.g., supercells produced all $\geq$ 2-in. diameter hail in RB98) or large sample sizes but no explicit information regarding storm type (Craven and Brooks 2004). More recent work by Thompson et al. (2003; hereafter T03), Davies (2004), Thompson et al. (2007, hereafter T07), and Davies and Fischer (2009) used hourly Rapid Update Cycle (RUC) model (Benjamin et al. 2004) analysis profiles to represent the near-storm environment associated with radar-identified supercells and other storm types. These studies provided valuable information regarding storm environment, especially with respect to supercells and tornado production, yet they focused on specific events or storm modes, and the sample sizes were too small to make any definitive statements regarding the frequency of occurrence of different storm modes. The importance of the convective mode is illustrated by the findings of Schoen and Ashley (2011) regarding U.S. fatalities with convective windstorms.

Trapp et al. (2005) developed a relatively large sample of convective modes [quasi-linear convective system (QLCS), discrete cell, and other] associated with tornadoes from 1999 to 2001 across the contiguous United

Corresponding author address: Richard L. Thompson, NOAA/NWS/NCEP/Storm Prediction Center, Ste. 2300, 120 David L. Boren Blvd., Norman, OK 73072.
E-mail: richard.thompson@noaa.gov

DOI: 10.1175/WAF-D-11-00116.1

States (CONUS), using regional radar reflectivity mosaics of relatively coarse spatial (2 km) and temporal (30 min) resolution. Somewhat more detailed convective mode categorizations were documented by Gallus et al. (2008) for a 10-state region in the summer, and this was followed by Duda and Gallus (2010) for the same region, with the addition of an estimate of supercell occurrence. These studies cataloged a larger number of convective mode cases than the prior proximity sounding work such as T07 and Davies and Fischer (2009), but they did not consider environmental information. Grams et al. (2012), however, combined a simplified convective mode classification scheme with RUC model and Storm Prediction Center (SPC) mesoanalysis environmental information to examine near-storm convective parameters in comparison to established severe weather ''checklist'' variables dating back to the 1950s.

In Part I of this study, Smith et al. (2012, hereafter S12) document the development of a large (22 901) sample of convective mode cases associated with tornadoes, ≥2-in. hail (hereafter sighail), and ≥65-kt (33 m s^{-1}) convective wind gusts (hereafter sigwind) across the CONUS. Volumetric Weather Surveillance Radar-1988 Doppler (WSR-88D) data were examined for all of the tornado, sighail, and sigwind events in an effort to assign a convective mode to each event for the period 2003–11. Please refer to S12 for additional details regarding the convective mode classification scheme.

Building on the work of S12, we have included near-storm environmental information associated with each severe storm and convective mode case. The long-term goal of the larger project is to provide representative samples of all significant severe storm events, along with respective convective modes and environmental information. Near-storm environments with supercell and QLCS tornadoes are the specific focus of this work, given that environmental information can be combined with storm mode information to improve the diagnoses and short-term watches and warnings of tornadoes and other significant severe thunderstorm events. Additional information specific to tropical cyclone tornadoes is presented in Edwards et al. (2012). In the following section, the data collection and methods are described, and in section 3 an analysis is presented of convective modes and environmental information focusing on tornadoes. Section 4 summarizes the findings of this work and outlines continuing and future work related to the SPC convective database.

2. Data and methods

All tornado, sighail, and sigwind reports for the period 2003–11 were filtered for the largest magnitude report per hour on a 40-km spacing RUC model analysis grid, and the time filtering assigned each report to the closest prior analysis hour. Tornado segment data (i.e., tornado damage paths broken down by individual tornadoes and counties) were used in order to provide higher tornado damage intensity resolution for long-track tornadoes, given damage ratings for each segment. This filtering procedure produced a sample of 22 901 severe thunderstorm grid-hour events, including 10 753 tornadoes, and 7495 sigwind and 4653 sighail events. The hourly RUC analysis grids form the foundation of the SPC mesoanalysis system (Bothwell et al. 2002), where hundreds of sounding-derived parameters are calculated at each analysis grid point. The RUC analyses at the lowest model level are used as a first-guess field in an objective analysis of the hourly surface observations, but no further modification of the model profiles is attempted. A subset of these convective parameters is archived[1] at the SPC (e.g., Schneider and Dean 2008), and these data provide the basis for the analyses herein.

One of the following three major convective mode classes was assigned to each tornado and significant severe thunderstorm event per S12: QLCS, right-moving (cyclonic) supercells (RMs) or left-moving (anticyclonic) supercells, and disorganized (cells and clusters clearly not meeting QLCS or supercell criteria). Subclassifications of each major category were as follows: QLCS included nonsupercell line and bow echo; supercell included discrete cell, cell in cluster, and cell in line; and disorganized included discrete cell, cell in cluster, and cluster. Two additional subsets consisted of storms with marginal supercell characteristics (after T03), and a linear hybrid mode with mixed characteristics of both line RM and QLCS (see S12 for a more detailed discussion regarding the practical difficulties of convective mode categorization). The derived parameters from the SPC mesoanalysis system were determined for each severe weather report and associated convective mode, forming the equivalent of a large close proximity sounding database for known storm types and severe weather events.

Data accuracy and representativeness

As with any attempt at assigning single point variables to represent a storm environment, concerns regarding the accuracy and representativeness of the data must be considered. Brooks et al. (1994) discussed many of the

[1] The date a parameter was first calculated as part of the SPC mesoanalysis system and occasional daily disruptions both affected the length of the archive for each parameter, such that a particular parameter may not have been available for the entire 2003–10 period of study (cf. sample sizes in Figs. 1 and 2).

concerns with arriving at ''proximity'' for a storm environment, while Potvin et al. (2010) considered the impacts of varying proximity criteria. Compared to rawinsonde observations, the SPC mesoanalysis system has the advantage of producing hourly environmental information on a 40-km spacing grid, which provides much greater spatial and temporal resolution than does the observed sounding network. The background RUC analyses incorporate a wide range of synoptic (e.g., standard 0000 and 1200 UTC rawinsonde observations) and asynoptic data (e.g., surface mesonet data, aircraft observations, etc.) to provide a reasonably accurate depiction of the synoptic and mesoscale environment, without the specific influence of the individual storms.[2] The most consistent biases noted by T03 in the RUC profiles were near the ground, where the SPC mesoanalysis system performs an objective analysis of the actual surface observations using the RUC analysis as a first-guess field. The result is an hourly surface analysis that attempts to remove RUC biases at the surface.

The SPC mesoanalysis approach does not correct for all potential errors. Given the propensity for severe thunderstorms to occur in the vicinity of baroclinic zones with strong horizontal gradients of temperature, moisture, and wind, small phase errors can result in somewhat misleading information for a particular storm case (e.g., 2100 UTC environmental data are assigned to a 2145 UTC tornado, but warm frontal passage was not reflected at the same grid point until the 2200 UTC analysis). In other cases, aspects of the background RUC analyses aloft may be questionable. The Greensburg, Kansas, tornado case, which was rated as a category 5 event on the enhanced Fujita scale (EF5), provides a specific example of this type of problem. The nearest RUC grid point profiles were apparently too dry just above the surface, and this strongly impacted parameters such as the lowest 100-mb mean-layer CAPE (MLCAPE) compared to the surface-based (SB) parcel counterpart (e.g., MLCAPE of 883 J kg^{-1} versus SBCAPE of 3487 J kg^{-1}). Though we have made no attempt to correct any individual errors, the experience of the authors in utilizing the mesoanalysis fields in operational practice and the prior work by T03 suggest that a very large sample size should minimize the impact of outliers within the sample.

All of the tornado cases were sorted initially by convective mode in order to provide an overview of environmental conditions related to each convective mode type. While a full spectrum of convective modes was documented, most of the archived mesoanalysis parameters are related primarily to supercells and tornadoes. Thus, the main focus of this study concerns tornado and significant tornado (e.g., ≥EF2 damage,[3] hereafter sigtor) production with RM storms, and a comparison of the supercell-related parameters to QLCS and other convective mode environments.

An ingredients-based approach (McNulty 1978, 1985; Doswell 1987; Johns and Doswell 1992) was applied in the diagnostic evaluation of the storm environments. The individual parameters can be grouped into measures of vertical wind shear, such as 0–1-km storm-relative helicity [SRH; Davies-Jones et al. (1990); using the storm motion estimate described by Bunkers et al. (2000)], and 0–6-km (all heights AGL) bulk wind difference (BWD; the magnitude of the vector wind difference between the top and bottom of the layer, as in T03). Two of the aforementioned vertical wind shear parameters have been modified to apply to a wide range of storm environments via an application of the ''effective inflow layer'' technique described in T07. The effective inflow base is defined as the first lifted parcel level that results in CAPE ≥ 100 J kg^{-1} and convective inhibition > -250 J kg^{-1}, and the top of the effective inflow layer is the last contiguous lifted parcel (working upward) to meet the same criteria. The so-called effective SRH (ESRH) is calculated using the bounds specified by the effective inflow layer. Moreover, the effective inflow base also serves as the beginning point in calculations of the effective bulk wind difference (EBWD), with the top of the EBWD layer defined as 50% of the vertical distance between the effective inflow base and the height of the equilibrium level for the most-unstable lifted parcel. The current SPC environmental archive only includes 0–6-km BWD and EBWD, although future versions of this database will likely include other measures of vertical wind shear, such as the 0–5-km layer advocated by Houston et al. (2008).

The SPC archive also includes thermodynamic parameters such as MLCAPE [using the virtual temperature correction described in Doswell and Rasmussen (1994)] and lifting condensation level (MLLCL). Combinations of the aforementioned vertical wind shear and thermodynamic parameters have been shown to discriminate most strongly between nonsupercells and

[2] Since 2010, the RUC has assimilated radar reflectivity and lightning through the diabatic digital filter initialization (see Benjamin et al. 2004), which indirectly includes convective storms in the initialization process.

[3] We refer to EF-scale damage ratings for all tornadoes, though the enhanced Fujita scale was not implemented until February 2007. The F-scale tornado damage ratings in prior years correspond to the same numerical rating in the EF scale for the same type of damage, though the EF scale includes more specific damage indicators.

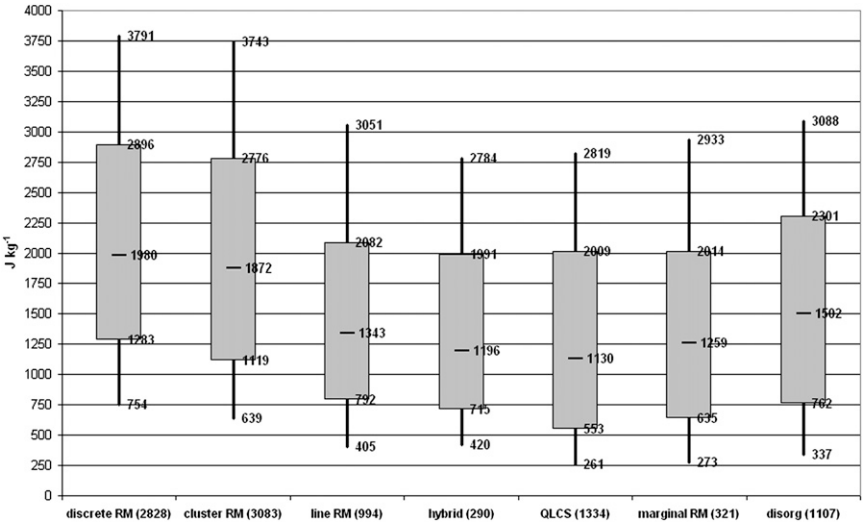

FIG. 1. Box-and-whiskers plot of MUCAPE (J kg^{-1}; sample period 2003–11) for the tornadoes and associated convective modes, where cases with hybrid characteristics of both line RMs and QLCSs are denoted as hybrid, and discrete cells/clusters with no organized structures are denoted as disorg. The shaded boxes span the 25th–75th percentiles, and the whiskers extend upward to the 90th and downward to the 10th percentiles. Median values are marked within the box, and sample sizes for each storm mode are shown in parentheses.

supercells [i.e., the effective-layer supercell composite parameter (SCP; Thompson et al. 2004)], and between nontornadic and significantly tornadic supercells [i.e., the significant tornado parameter (STP; T03)].

The original version of the STP presented in T03 was modified as of March 2005 to include the effective-layer vertical wind shear parameters, along with convective inhibition:

$$\text{effective-layer STP} = \{(\text{MLCAPE}/1500\,\text{J kg}^{-1}) \times (\text{ESRH}/150\,\text{m}^2\,\text{s}^{-2}) \times (\text{EBWD}/20\,\text{m s}^{-1}) \times [(2000 - \text{MLLCL})/1000\,\text{m}] \times [(200 + \text{MLCIN})/150\,\text{J kg}^{-1}]\},$$

where the EBWD term is capped at a value of 1.5 for EBWD > 30 m s^{-1}, and set to 0.0 for EBWD $<$ 12.5 m s^{-1}; the MLLCL term is set to 1.0 for MLLCL heights $<$ 1000 m AGL, and set to 0.0 for MLLCL heights $>$ 2000 m AGL; and the MLCIN term is set to 1.0 for MLCIN > -50 J kg^{-1}, and set to 0.0 for MLCIN < -200 J kg^{-1}.

It is important to understand the limitations of convective parameters and indices (Doswell and Schultz 2006) since they compose the majority of our database. Specific concerns include the choice of lifted parcels and details in the vertical moisture profiles that impact CAPE and effective inflow-layer calculations, or estimated

TABLE 1. Mean (median) values of the effective-layer SCP and its three components across four tornadic convective mode subsets. Convective mode conventions are the same as in Fig. 1.

	Discrete RM	Line RM	QLCS	Disorg
MUCAPE (J kg^{-1})	2167 (1980)	1559 (1343)	1381 (1130)	1643 (1502)
EBWD (kt)	50 (49)	50 (51)	42 (44)	25 (23)
ESRH (m^2 s^{-2})	261 (223)	295 (279)	230 (181)	68 (35)
SCP	10.7 (8.3)	9.2 (7.6)	6.2 (4.0)	1.9 (0.1)

TABLE 2. Mean differences in the effective-layer SCP and its three components across four tornadic convective mode subsets. Convective mode conventions are the same as Table 1, including parameter units. Boldface differences are statistically significant at $\alpha < 0.001$, and boldface and italic differences are considered to be sufficiently large to be of operational significance.

	Discrete RM − line RM	Discrete RM − QLCS	Line RM − QLCS	Discrete RM − disorg
MUCAPE	***607***	***786***	**178**	***523***
EBWD	−1	**7**	**8**	***25***
ESRH	**−34**	**30**	**65**	***192***
SCP	**1.4**	***4.5***	***3.1***	***8.7***

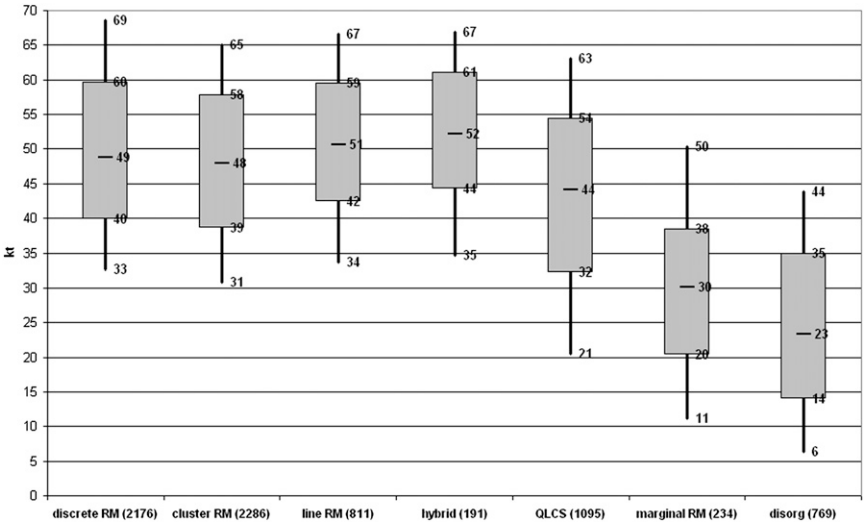

FIG. 2. As in Fig. 1, but for the EBWD (kt; sample period March 2005–11).

storm motion errors and resultant variations in SRH. Any errors in the individual parameters carry over to the combined indices (SCP and STP) in a nonlinear manner. Fortunately, these concerns can be alleviated somewhat by very large sample sizes, as well as previous work supporting the statistical ability of the composite parameters to discriminate between tornadic and nontornadic supercells (e.g., RB98 and T03, among others).

Severe thunderstorms that produced hail <2-in. (5.1 cm) diameter hail or wind gusts <65 kt (33 m s^{-1}) were not part of this database, nor were nonsevere thunderstorms due to an unmanageably large number of such cases for manual convective mode classification. The exclusion of these weaker events precludes a complete assessment of null cases for each event type. Instead, comparison null-tornado samples were identified by applying standard proximity sounding criteria [e.g., ±3 h and within 185 km per Craven and Brooks (2004)] to each event type, leaving a subset of sighail and sigwind events with no nearby tornadoes.

3. Results and discussion

a. *Tornado environments by convective mode and EF-scale damage rating*

Tornadoes of all damage class ratings composed 10 753 of the 22 901 convective mode cases in the 9-yr sample across the CONUS (see Table 1 from S12 for detailed information regarding the distribution of specific

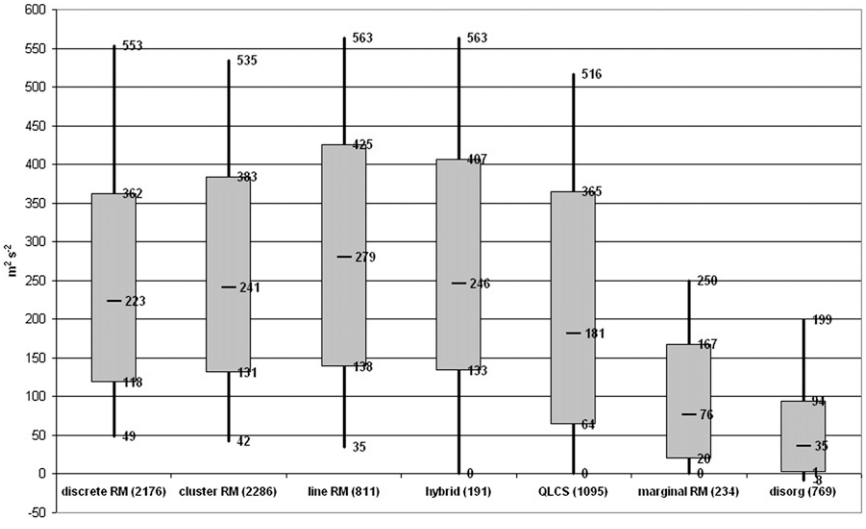

FIG. 3. As in Fig. 1, but for ESRH (m^2 s^{-2}; sample period March 2005–11).

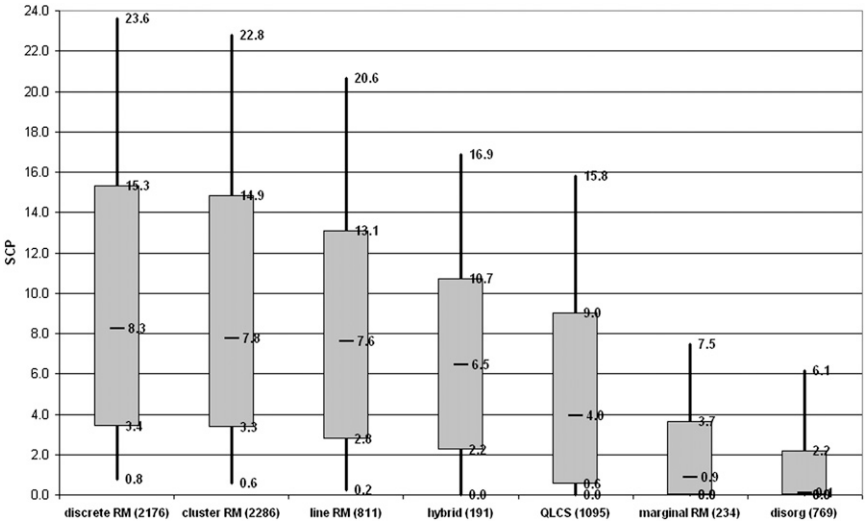

FIG. 4. As in Fig. 1, but for effective-layer SCP (dimensionless; sample period March 2005–11).

convective modes). Over the entire sample of tornado events, most-unstable parcel CAPE (MUCAPE; Doswell and Rasmussen 1994) spanned a rather wide range from less than 500 J kg^{-1} on the low end (i.e., 10th percentile bottom whiskers in Fig. 1) to in excess of 3500 J kg^{-1}. The tornadic linear convective modes (line RM and QLCS) were associated with somewhat lesser MUCAPE compared to discrete RM and cluster RM, but with substantial overlap between mode types within the parameter space. Differences in mean MUCAPE values exceeded 600 J kg^{-1} between discrete RM and linear tornado events (Tables 1 and 2), and these results were statistically significant at $\alpha < 0.001$ for a two-tailed t test with unequal variances (Wilks 1995). Overall, the results presented herein confirm the findings of previous observational proximity sounding studies (e.g., RB98; Craven and Brooks 2004) in that there is large overlap in the CAPE distributions for all of the storm classes, and CAPE itself is not a particularly good discriminator between tornadic storm modes across all seasons combined.

Environmental influences on storm mode become more apparent when considering EBWD and ESRH (Figs. 2 and 3, respectively). Organized severe storm

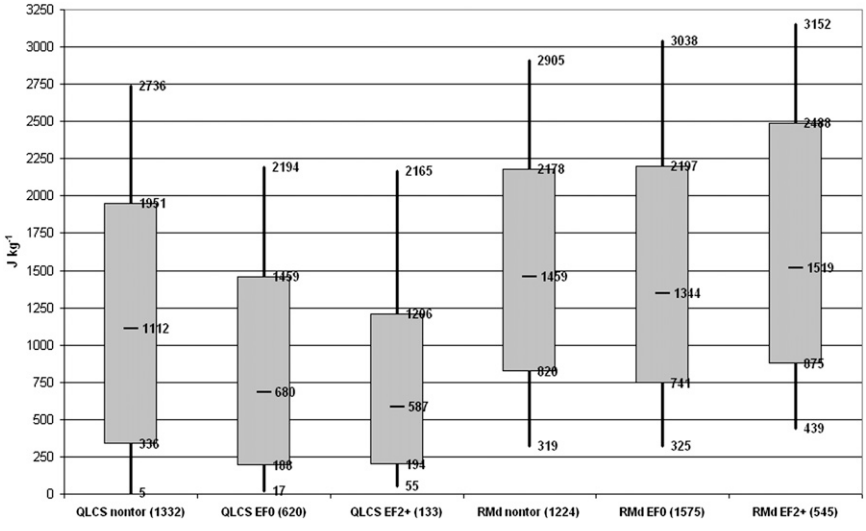

FIG. 5. Box and whiskers plot of MLCAPE (J kg^{-1}; sample period 2003–11) for nontornadic (nontor), weak tornado (EF0), and significant tornado (EF2+) events associated with QLCSs and discrete RMs (denoted RMd). Other conventions are the same as in Fig. 1.

TABLE 3. Mean (median) values of the effective-layer STP and its five components across three tornado damage classes (EF2 represents all sigtor events) of discrete RMs (RMd) and QLCSs. The RMd nontor and QLCS nontor categories consist only of sighail and sigwind events, with no tornado reports within ±3 h and 185 km. Other conventions are the same as in Table 1.

	RMd EF2	RMd EF0	RMd nontor	QLCS EF2	QLCS EF0	QLCS nontor
MLCAPE (J kg^{-1})	1705 (1519)	1561 (1344)	1578 (1459)	855 (587)	923 (680)	1261 (1112)
|MLCIN| (J kg^{-1})	47 (28)	55 (31)	91 (53)	85 (58)	77 (51)	125 (84)
MLLCL (m AGL)	955 (875)	1147 (1053)	1424 (1364)	896 (763)	938 (855)	1114 (1028)
EBWD (kt)	57 (58)	46 (45)	44 (44)	47 (49)	39 (39)	35 (35)
ESRH (m^2 s^{-2})	381 (362)	206 (176)	131 (110)	296 (291)	199 (139)	132 (100)
STP	3.3 (2.3)	1.4 (0.7)	0.6 (0.2)	1.2 (0.6)	0.8 (0.2)	0.5 (0.0)

modes such as RM and linear hybrids resided within the parameter space associated with supercells in previous studies [e.g., EBWD > 30–40 kt (15–20 m s^{-1}) per Fig. 2 and T07], whereas a gradual decrease in vertical shear was observed in the transition from QLCS to marginal RM and disorganized storms. The EBWD appears to provide the strongest discrimination between the classes of RM and the disorganized tornadic storm modes. Combining the ingredients into the SCP reveals a similar decrease in values from the RM down to QLCS and disorganized storms (Fig. 4). The most substantial differences in storm environments occurred for EBWD and ESRH between discrete RM and disorganized tornadic storms, while MUCAPE discriminates marginally between either discrete RM or cluster RM and linear tornado events (line RM and QLCS). Differences in low-level and deep-layer vertical shear (e.g., ESRH and EBWD, respectively) between RM and QLCS environments were too small to be of practical utility in an operational forecasting environment, despite statistical significance in the difference of the means (e.g., Potvin et al. 2010). The linear hybrid events, with a mix of radar-identifiable RM and QLCS characteristics, generally fell between or were similar to the parameter distributions with line RM and QLCS (Figs. 1–4).

The tornado event sample was also sorted to identify variations in storm environments with specific convective modes across tornado damage ratings. As seen in Fig. 5 and Tables 3 and 4, MLCAPE with sigtor discrete RMs exceeded QLCS events by roughly 500 J kg^{-1}, although no meaningful differences in MLCAPE were noted across the EF-scale damage ratings within either mode category. Interestingly, 45% of the QLCS tornado events were associated with MLCAPE < 500 J kg^{-1}, compared to only 15% of discrete RM tornado events. The opposite trends were noted with MLLCL heights (Fig. 6), with smaller ranges and more moist low-level environments for the significant tornadoes with both RM and QLCS events, and drier environments and wider ranges of values for the nontornadic storms. The largest LCL heights accompanied the subset of nontornadic discrete RMs that produced primarily sighail (RMd nontor in Fig. 6); these storms were largely confined to the Great Plains. MLCIN displayed some differences between storm modes, where the smallest MLCIN magnitudes (a majority < 50 J kg^{-1}) were associated with the tornadic discrete RMs, while the largest MLCIN magnitudes accompanied the nontor QLCS (Fig. 7).

Measures of deep-layer vertical shear discriminate well between discrete RM and nonsupercell storms (e.g., Weisman and Klemp 1982; RB98; T03; among others), but not particularly well between the same tornado damage classes of QLCSs and discrete RMs (Fig. 8). Differences between the sigtor discrete RM and the other RM/QLCS categories are more pronounced when considering the EBWD, which accounts for the depth of buoyancy. The 0–6-km BWD shows the smallest overlap between the sigtor QLCS and nontor QLCS (compared to EBWD), which reflects the stronger vertical shear environments of the QLCS sigtor events, regardless of

TABLE 4. Mean differences in the effective-layer STP and its five components across seven convective mode subsets. Other conventions are the same as in Table 3.

	RMd EF2 − RMd EF0	RMd EF2 − RMd nontor	RMd EF2 − QLCS EF2	RMd EF2 − QLCS nontor	QLCS EF2 − QLCS EF0	QLCS EF2 − QLCS nontor	QLCS EF2 − RMd nontor
MLCAPE	144	126	***849***	***444***	−68	**−405**	***−723***
|MLCIN|	−8	***−45***	**−38**	***−78***	8	**−40**	−6
MLLCL	**−192**	***−469***	59	**−159**	−42	**−218**	***−528***
EBWD	***11***	***13***	***10***	***22***	**9**	**13**	4
ESRH	***175***	***250***	**85**	***250***	***97***	**165**	***165***
STP	***1.9***	***2.7***	***2.1***	***2.8***	0.4	**0.7**	**0.6**

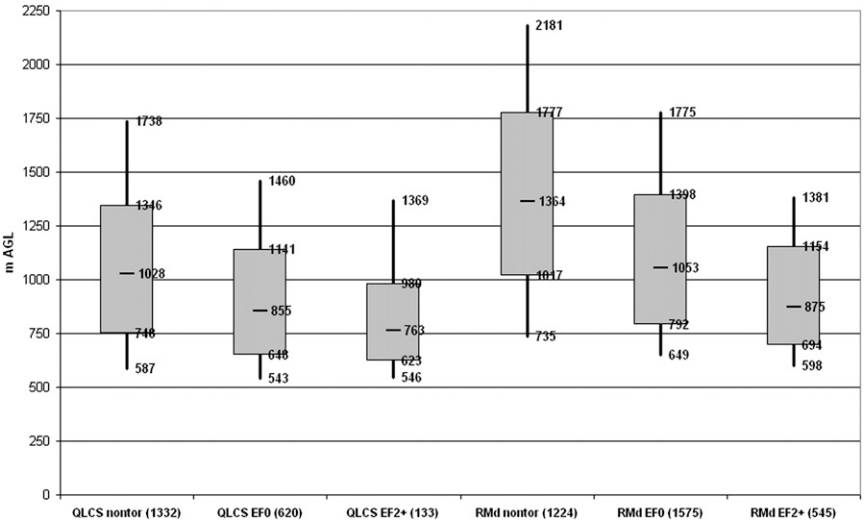

FIG. 6. As in Fig. 5, but for MLLCL height (m AGL; sample period 2003–11).

storm depth. The lowest quartiles of nontornadic and EF0 QLCS events fall below the range of EBWD and 0–6-km BWD typically associated with right-moving supercells.

Measures of low-level vertical wind shear show greater discrimination between the tornado damage rating classes for both QLCS and RM, compared to EBWD and 0–6-km BWD. This is consistent with many previous studies. The differences in 0–1-km SRH between the nontor discrete RM and the sigtor discrete RM (Fig. 9) were quite pronounced, with a large majority of sigtor (nontor) cases having both 0–1-km SRH and ESRH greater (less) than 200 $m^2 s^{-2}$. In agreement with the previous work of Markowski et al. (2003) and Craven and Brooks (2004), a similar signal is noted in Fig. 10 with 0–1-km BWD at a threshold in the range of 20–30 kt (10–15 m s^{-1}). This measure of fixed-layer vertical wind shear may be more appropriate for a RM and QLCS tornado environment comparison since, unlike SRH, it does not rely on an assumed RM storm motion. Still, the 0–1-km SRH, ESRH, and 0–1-km BWD do not provide effective differentiation between the same tornado damage class ratings of QLCS and RM.

b. Variations in EF-scale damage by environment, storm mode, and mesocyclone strength

Both the sigtor QLCS and sigtor discrete RMs occur in the strongest vertical shear environments per Figs. 8–10,

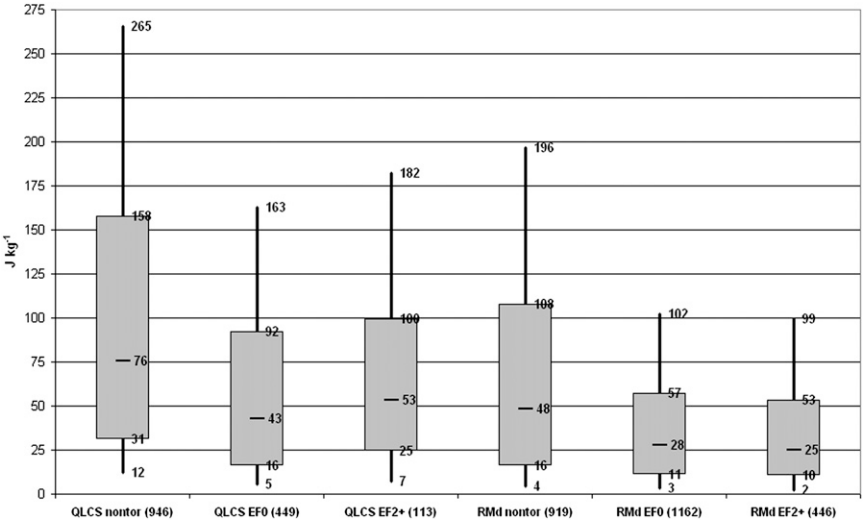

FIG. 7. As in Fig. 5, but for magnitude of MLCIN (J kg^{-1}; sample period March 2005–11).

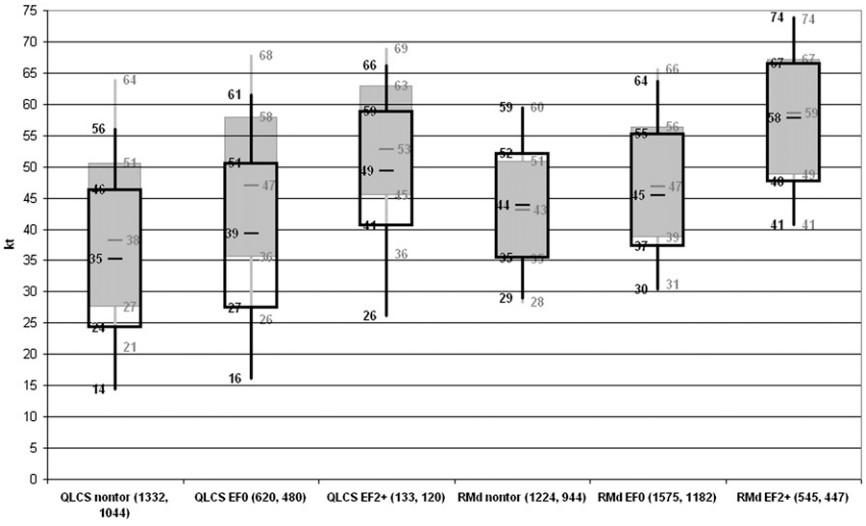

FIG. 8. As in Fig. 5, but for 0–6-km BWD (kt; shaded boxes with gray labels on the right; sample period 2003–11) and EBWD (kt; black overlays with black labels on the left; sample period March 2005–11).

while weaker instability distributions characterize QLCS events compared to all types of discrete RMs (Fig. 5). Differences in storm environments for the tornadic classes of QLCS and discrete RM become more apparent via the nonlinear combination of ingredients in the effective-layer STP (Fig. 11). The sigtor discrete RMs reside in the most volatile combinations of buoyancy and vertical shear, much higher in the parameter space than either of the nontornadic storm samples, and noticeably greater than the tornadic QLCS and weakly tornadic (EF0 damage) RM distributions.

The STP was designed to identify the most dangerous supercell tornado environments, yet relatively small sample sizes in prior studies (i.e., T03) precluded examination of STP as a function of EF-scale tornado damage with supercells. In Fig. 12, a monotonic increase in effective-layer STP is noted with increasing EF-scale damage ratings for all damage classes and at all percentile ranks, where larger values of STP correspond to more intense tornado damage on average. Not only do point values of effective-layer STP closest to the events increase for increasing EF-scale damage ratings, but

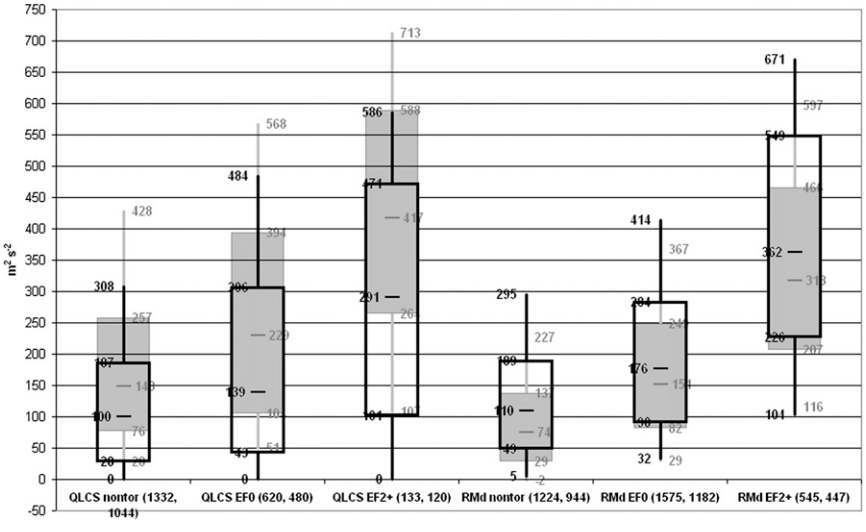

FIG. 9. As in Fig. 5, but for 0–1-km SRH ($m^2\ s^{-2}$; shaded boxes with gray labels on the right; sample period 2003–11) and ESRH ($m^2\ s^{-2}$; black overlays with black labels on the left; sample period March 2005–11).

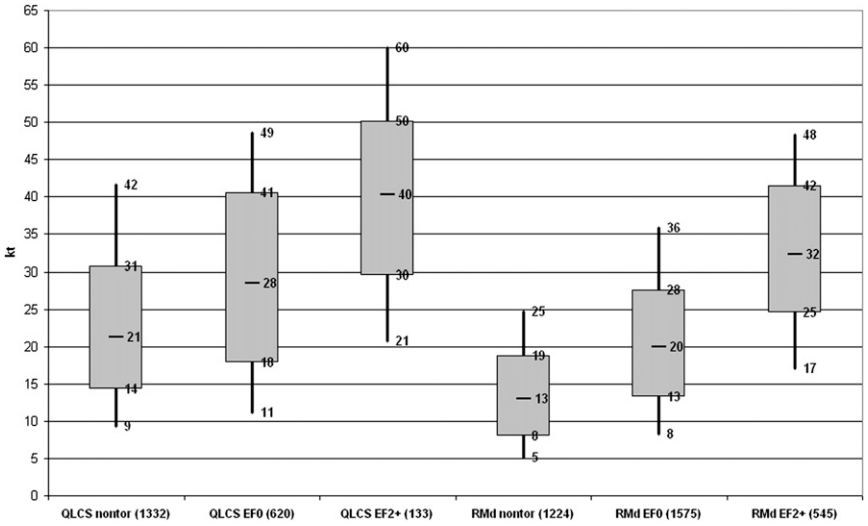

FIG. 10. As in Fig. 5, but for 0–1-km BWD (kt; sample period 2003–11).

regional peak values of effective-layer STP in proximity to the storm events show the same trend at larger magnitudes (e.g., overlay in Fig. 12). This is consistent with the results of Cohen (2010), who found that significant tornadoes rarely occur in the STP maximum, and are instead often found on the spatial gradient. The relative frequency of RM tornadoes increases in each EF-scale damage category with increasing STP (Table 5), with much higher relative frequencies of larger effective-layer STP values for the EF4+ tornadoes. Still, weaker RM tornadoes dominate the overall frequency distribution across nearly all values of effective-layer STP since the weakest tornado events with corresponding archived environmental data (2693 EF0) far outnumber the most intense tornadoes (71 EF4–EF5). The substantial overlap in the STP distributions (Fig. 12) and the tendency for weak tornadoes to far exceed the number of intense tornadoes suggest that confident delineation in damage categories will prove difficult for individual storms during a particular hour, based on storm mode and environment alone. However, Fig. 12 suggests that a rough effective-layer STP threshold of ≥ 1 discriminates between the sigtor and nontor events at the grid point closest to each event. Likewise, the regional (within 185 km) maximum

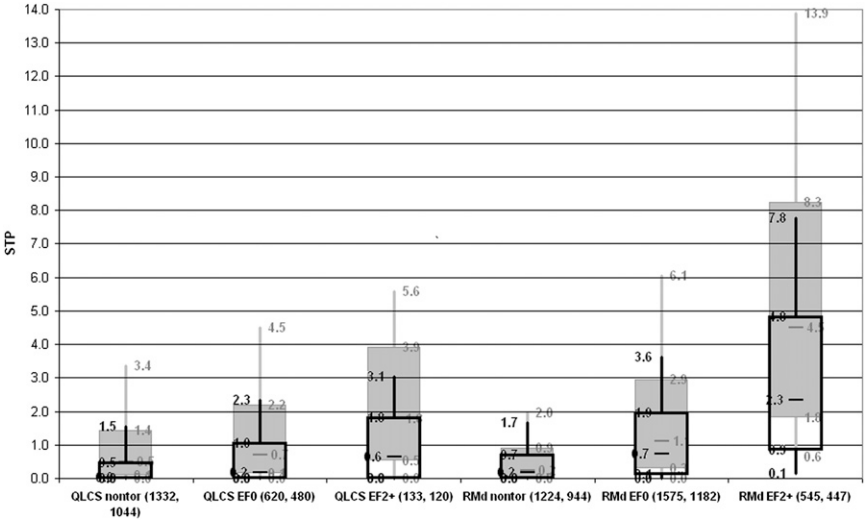

FIG. 11. As in Fig. 5, but for the original T03 version of STP (dimensionless; shaded boxes with gray labels on the right; sample period 2003–11) and effective-layer STP (dimensionless; black overlays with black labels on the left; sample period March 2005–11).

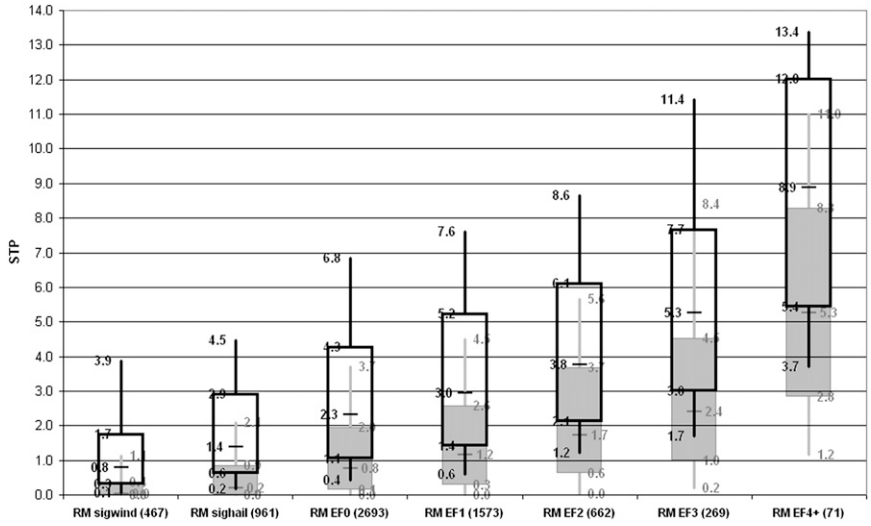

FIG. 12. Box-and-whiskers plot of effective-layer STP (dimensionless; sample period March 2005–11) for all RMs by EF-scale damage rating classes (shaded gray, labels on right), including nontornadic RMs that produced only sigwind or only sighail. Black overlays (labels on left) denote maximum STP values within 185 km (100 n mi) of each event grid point, at the analysis time immediately preceding the event time. Other conventions are the same as in Fig. 1.

values of effective-layer STP ≥ 2 correspond to the EF3+ tornado events, compared to RMs that produced only sigwind or sighail.

Manual estimates of mesocyclone strength were determined for all of the supercells (cyclonic for the RMs and anticyclonic for the left-moving supercells), following the mesocyclone nomograms developed by the Warning Decision Training Branch of the National Weather Service [after Andra (1997) and Stumpf et al. (1998)]. The mesocyclone strengths appear to be related to the storm environment, as represented by the SCP for the three rotational strength categories shown in Fig. 13. The stronger mesocyclones occurred more commonly in the environments more favorable for RM (i.e., larger SCP). A comparison of effective-layer STP to EF scale for RMs (Fig. 14) reveals the combined tendency for the more intense (EF3+) tornadoes to occur primarily with strong mesocyclones in environments of relatively large STP, while the RMs with weak mesocyclones occur in somewhat marginal environments and produce very few EF3+ tornadoes.

Although the primary value of the STP is in identifying juxtapositions of important supercell tornado ingredients, the individual components in the STP should always be examined independently to ascertain the relative contributions of each component. The instability and vertical shear parameters examined herein do show some ability to discriminate between the sigtor RM and QLCS events; however, accurate forecasts of convective mode are still necessary since most EF3+ tornadoes (86%) occur with discrete or cluster RMs (Table 2 in S12). Dial et al. (2010) found that the strength of the low-level forcing for ascent, the orientation of deep-layer shear vectors relative to initiating synoptic boundaries, and the motions of individual storms relative to boundary motion hold promise in delineating between linear and discrete convective modes—in environments otherwise supportive of supercells.

c. *Seasonal variations in sigtor RM and tornadic QLCS environments*

Seasonal dependencies in both convective mode distributions (e.g., Figs. 11 and 12 from S12) and environmental parameters provide the motivation for seasonal breakdowns in tornado environments by convective

TABLE 5. Cumulative frequency of effective-layer STP (columns) by tornado EF-scale damage (rows) for all RMs. Cumulative frequencies are denoted by regular (0%–24%), italic (25%–49%), boldface (50%–74%), and boldface italic (≥75%). Nontornadic RMs produced either sigwind or sighail, with no duplication of grid points (i.e., sigwind and sighail assigned to the same grid point in the same hour), and no tornadoes within 185 km.

	<0.5	≥0.5	≥1.0	≥2.0	≥4.0	≥6.0	Total
Nontor	**0.67**	*0.33*	0.20	0.10	0.03	0.01	1966
EF0	*0.41*	**0.59**	*0.43*	*0.25*	0.09	0.03	2693
EF1	*0.31*	**0.69**	**0.54**	*0.33*	0.13	0.05	1573
EF2	0.22	***0.78***	**0.65**	*0.44*	0.23	0.09	662
EF3	0.16	***0.84***	***0.75***	**0.55**	*0.30*	0.16	269
EF4+	0.06	***0.94***	***0.92***	***0.83***	**0.66**	*0.42*	71

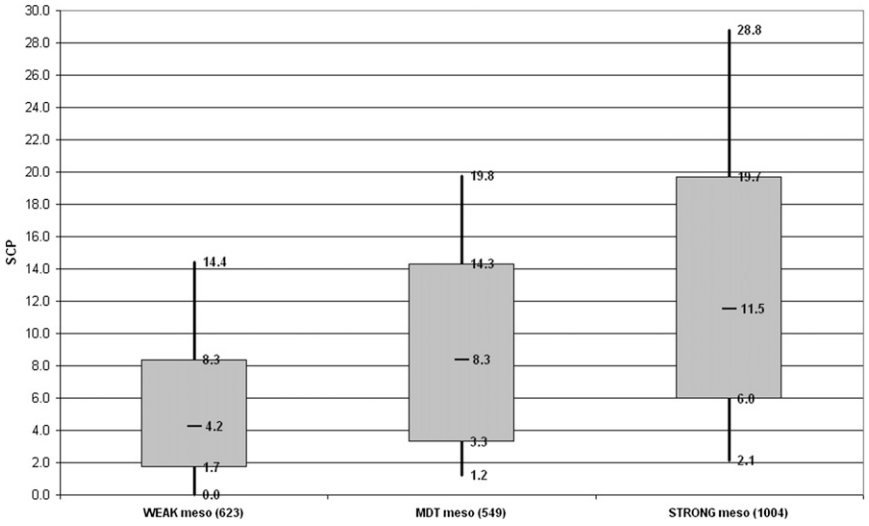

FIG. 13. Effective-layer SCP (dimensionless; sample period March 2005–11) with all tornadic discrete RMs for weak, moderate (MDT), and strong mesocylones. Box-and-whiskers conventions are the same as in Fig. 1.

mode. Seasonal geographic variations in sigtor RM distribution from S12 are shown in Fig. 15, with clustering of sigtor events across the lower Mississippi and Tennessee Valleys in the winter (December–February), the central Great Plains to the middle Mississippi Valley in the spring (March–May), the northern Great Plains in the summer (June–August), and the lower Ohio and Mississippi Valleys in the fall (September–November). However, for comparative purposes, only 119 sigtor QLCS events (with all accompanying environmental data) were observed in our sample, leading to small seasonal samples (26 winter, 72 spring, 14 summer, and 7 fall). These sample sizes were judged to be too small to warrant a robust statistical comparison with sigtor RMs across all four seasons; thus, all EF1+ QLCS tornado events were considered hereafter to allow similar

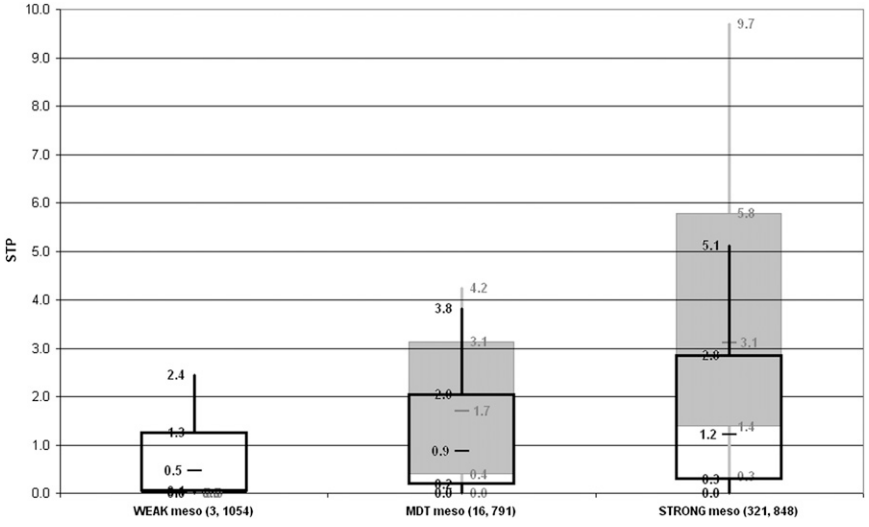

FIG. 14. As in Fig. 13, but for effective-layer STP (dimensionless; sample period March 2005–11). The shaded boxes (gray labels on the right) denote RMs with EF3+ tornado damage, and the black overlays (with labels on the left) represent the RMs that produced EF0 tornado damage. Sample sizes are denoted in parentheses, with the RM EF3+ tornadoes first and RM EF0 tornadoes second. The sample size for EF3+ tornadoes with weak mesocyclones was too small (three cases) to justify a box-and-whiskers plot.

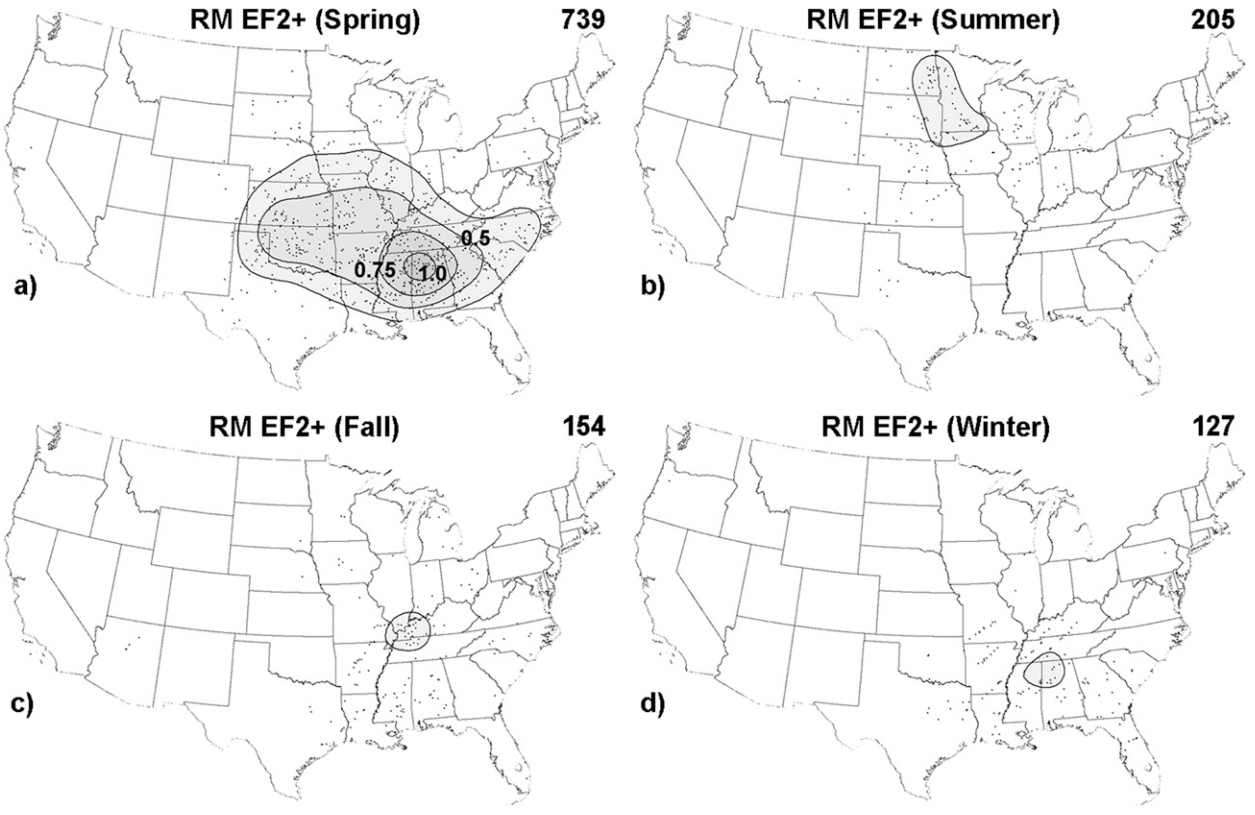

FIG. 15. Kernel density estimate on a 40-km spacing grid of all sigtor RM (excluding hybrid subcategory and tropical cyclone) tornado events (EF2–EF5) by season: (a) March–May (spring), (b) June–August (summer), (c) September–November (fall), and (d) December–February (winter). Black dots represent the individual sigtor events that formed the basis of the kernel density estimate. The minimum contour and shading begins at 0.25 events per 10-yr estimate based on 2003–10 data, while the labeled contours begin at 0.5 events per 10 yr. The numbers at the top right of each panel show the event count per season.

seasonal sample sizes. From Fig. 16, it is seen that QLCS tornado events exhibited similar seasonal variations, but at a lower frequency of occurrence compared to sigtor RM.

The supercell tornado ingredients also exhibited noteworthy seasonal and regional variabilities. Winter and fall MLCAPE values were substantially lower than spring and summer values (Fig. 17) for both sigtor RM and tornadic QLCS, with notably weaker buoyancy across all seasons for the tornadic QLCSs compared to the sigtor RMs. The largest relative seasonal difference was in the winter, where approximately 75% of the sigtor RMs occurred with MLCAPE > 350 J kg^{-1}, and approximately 75% of the tornadic QLCSs occurred with MLCAPE < 450 J kg^{-1}. MLLCL heights (Fig. 18) were similar in distribution to MLCAPE by season, with the highest values in the spring and summer, and the lowest values in the fall and winter. Unlike MLCAPE, both sigtor RMs and tornadic QLCSs occupied the same approximate range of the parameter space for MLLCL in the fall, winter, and spring. Lower LCL heights were observed with summer QLCS tornado events compared to summer RM sigtor events, which is primarily a reflection of lower surface temperatures (and similar dewpoint temperatures) in QLCS tornado environments compared to sigtor RM environments (not shown). Cooler surface temperatures (1°–2°C) across all seasons in QLCS tornado environments were also reflected in smaller MLCAPE (Fig. 18) and larger MLCIN values (Fig. 19).

Not surprisingly, vertical wind shear was strongest during the winter and transition seasons (Figs. 20 and 21) when events clustered from the central and southern Great Plains to the Deep South and lower Ohio Valley, compared to weaker vertical shear in the summer across the northern Great Plains. Both ESRH and EBWD tended to be weaker for QLCS EF1+ events compared to sigtor RMs in the transition seasons, and especially during the winter. A similar seasonal trend for weaker fixed-layer vertical shear is noted for both 0–1-km SRH and 0–6-km BWD (not shown). Differences between the effective-layer shear parameters and their fixed-layer

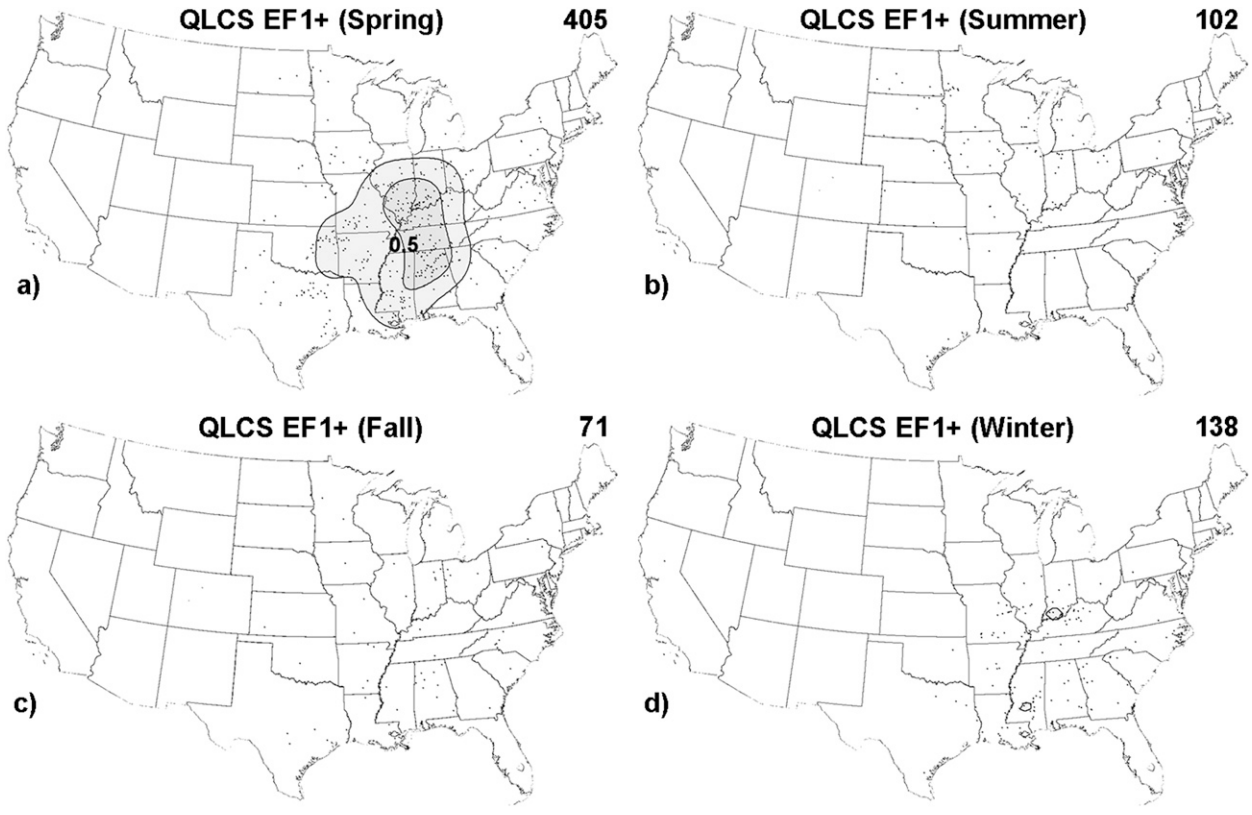

FIG. 16. As in Fig. 14, but for all EF1+ QLCS tornadoes (excluding hybrid subcategory and tropical cyclone).

counterparts were most pronounced when buoyancy was weakest in the winter with QLCS tornado events. The effective-layer shear values were weaker in the winter as a result of both shallower buoyancy (i.e., lower equilibrium level heights) and shallower effective inflow-layer depths. Conversely, the fixed-layer and effective-layer shear parameter distributions were quite similar in the summer, when buoyancy is strongest.

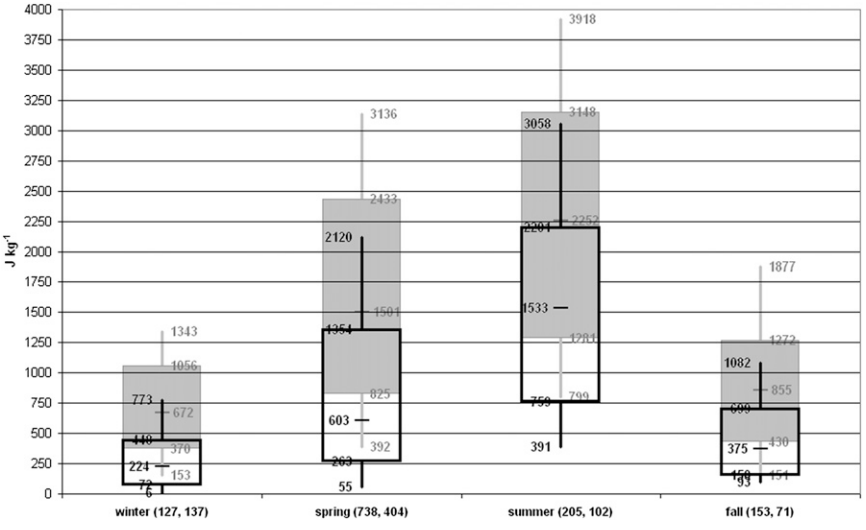

FIG. 17. Seasonal box-and-whiskers plot of MLCAPE (J kg^{-1}; sample period 2003–11) for all RMs that produced EF2+ tornadoes (shaded gray) and QLCSs with EF1+ tornadoes (black overlay). Sample sizes are denoted in parentheses with RM EF2+ tornadoes first and QLCS EF1+ tornadoes second. Other plot conventions are the same as in Fig. 8.

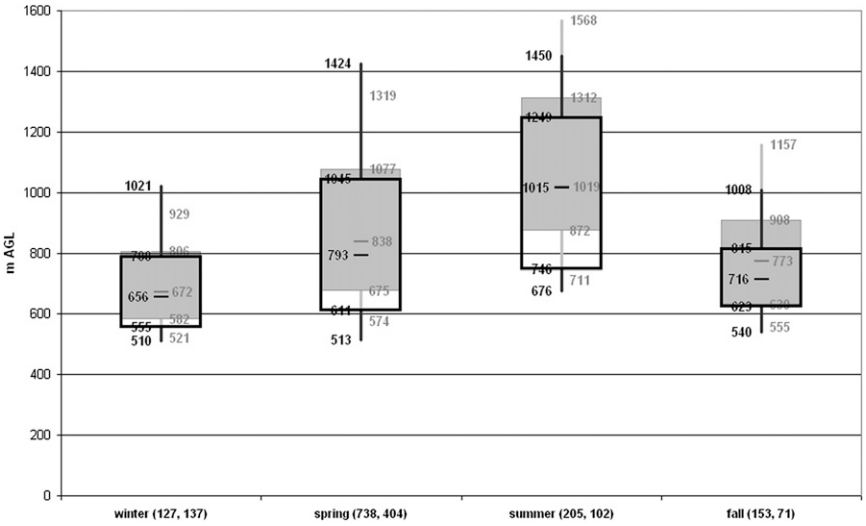

FIG. 18. As in Fig. 17, but for MLLCL height (m AGL; sample period 2003–11).

Shafer et al. (2010) found strong seasonal dependencies and poor discrimination skill in their nonoperational model forecasts of thermodynamic parameters such as surface-based CAPE and LCL height for tornado outbreaks and primarily nontornadic outbreaks; 0–1- and 0–3-km SRHs were more skillful discriminators and showed somewhat less seasonal dependence. Our results reflect the Shafer et al. (2010) findings in terms of the seasonal variations and poor discrimination between QLCS tornado events and sigtor RM events for MLLCL height, although similar seasonal dependencies and difficulties are noted with ESRH and 0–1-km SRH (not shown). Unlike Shafer et al. (2010), our MLCAPE samples (Fig. 17) suggest more substantial differences between tornado events by convective mode within each season, especially during the winter when buoyancy is weakest overall. These differences are likely the result of the different sampling criteria (i.e., their regional fields of model-predicted parameters in known severe weather outbreaks versus our near-storm diagnostic point values of similar parameters for specific convective modes in known tornado events) and goals (i.e., discrimination between forecasts of outbreak type versus diagnosis of near-storm environments by convective mode) in Shafer et al. (2010) compared to the current study, respectively.

The most important seasonal differences in sigtor RM versus tornadic QLCS environments can be summarized as follow:

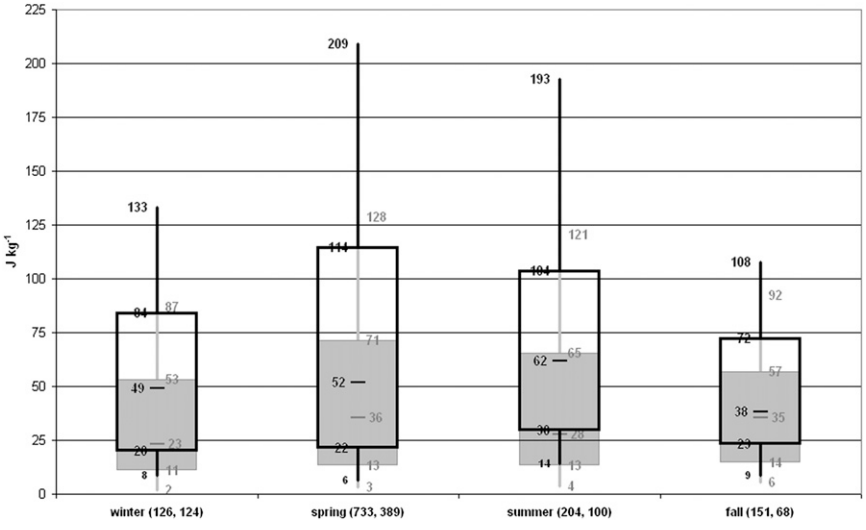

FIG. 19. As in Fig. 17, but for magnitude of MLCIN (J kg^{-1}; sample period March 2005–11).

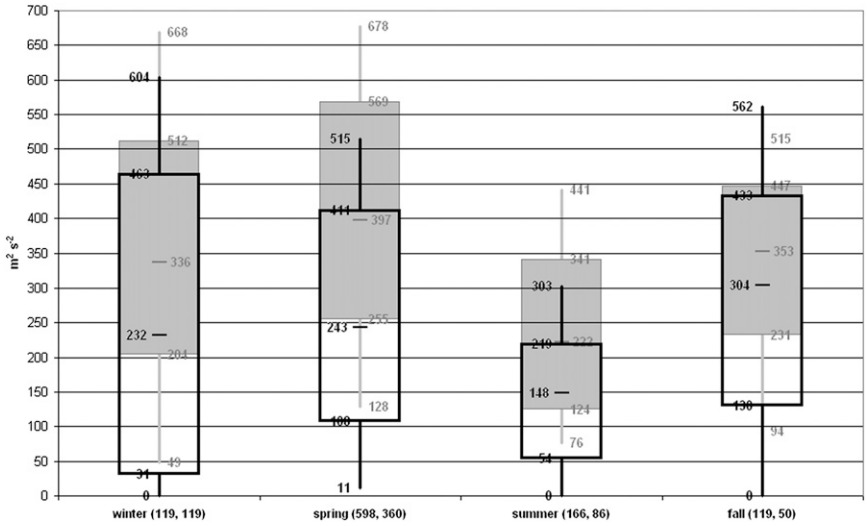

FIG. 20. As in Fig. 17, but for ESRH (m^2 s^{-2}; sample period March 2005–11).

1) Winter and fall QLCS tornadoes occurred in vertical shear environments (both effective layer and fixed layer) supportive of supercells, similar to the sigtor RM distributions.
2) A large majority of winter QLCS tornado environments were characterized by weak buoyancy (MLCAPE < 400 J kg^{-1}) compared to the sigtor RM.
3) Fixed-layer vertical shear was largest in the winter QLCS tornado events, but the weaker buoyancy contributed to reduce the effective-layer shear parameters compared to the fixed-layer shear parameters.
4) Summer QLCS tornadoes occurred with somewhat weaker buoyancy compared to sigtor RMs, and with both deep-layer and low-level vertical shears closer to the lower range for supercells.
5) Both buoyancy and effective-layer vertical shears were weaker in the spring QLCS tornado environments compared to the sigtor RM environments.

A combination of ingredients into the effective-layer STP (Fig. 22) highlighted the more dangerous spring environments across the Great Plains and Mississippi Valley, where sigtor RMs were most common. Notably, the spring environments did not display the largest MLCAPE, lowest MLLCL heights, or strongest vertical shear compared to the other seasons, but the spring had no consistent weakness in any of the ingredients, such as weaker buoyancy in the winter or weaker low-level shear in the summer. The effective-layer STP also discriminated reasonably well between the tornadic QLCS

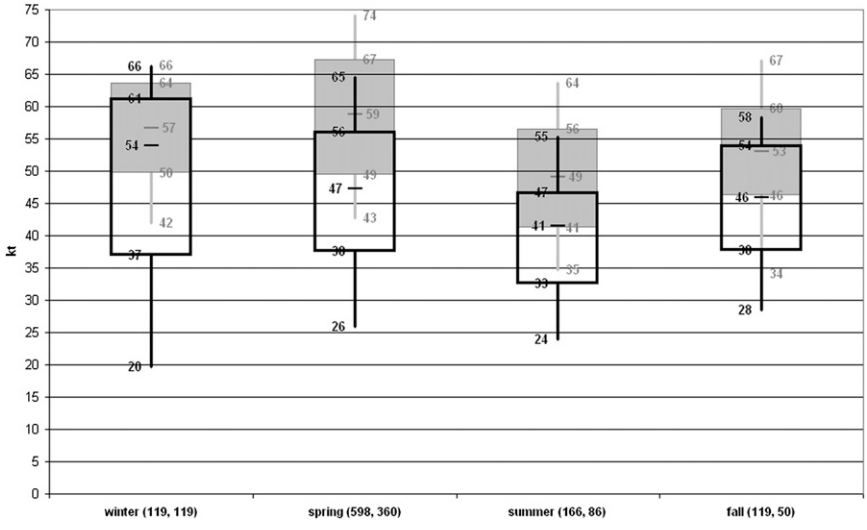

FIG. 21. As in Fig. 17, but for EBWD (kt; sample period March 2005–11).

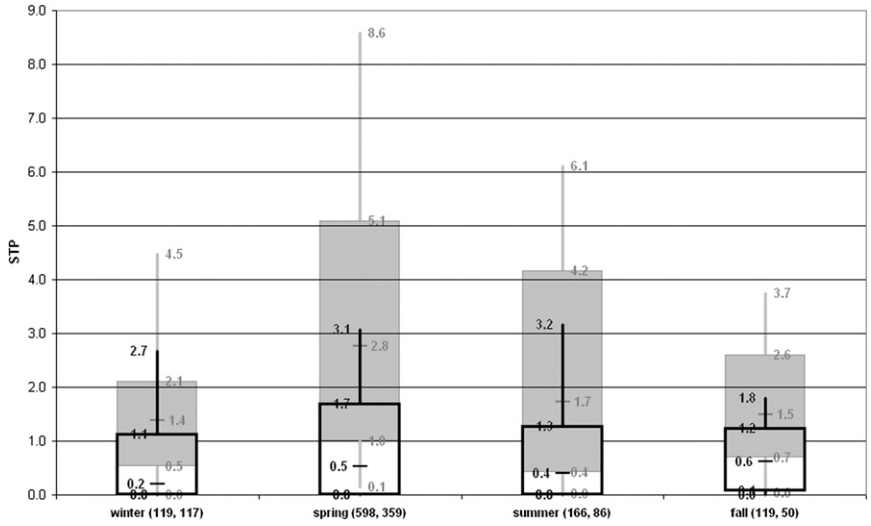

FIG. 22. As in Fig. 17, but for effective-layer STP (dimensionless; sample period March 2005–11).

and sigtor RM environments across the other seasons, with effective-layer STP ≤ 1 for a majority of QLCS tornadoes.

4. Summary and conclusions

The relational database of severe storm events and environmental parameters maintained at the SPC (Schneider and Dean 2008) has been augmented to include convective mode information for ~80% of all tornado and significant severe thunderstorm events from 2003 to 2011. The convective mode assignments were based on manual inspection of level II or level III WSR-88D imagery associated with the radar site closest to each event (S12). This resulted in the identification of 10 753 tornado, 7495 sigwind, and 4653 sighail events across the CONUS with associated convective mode and environmental information. The convective modes and environments associated with the tornado events were the focus of this work.

Right-moving supercells dominated tornado production within our sample, thus forming the core of the investigation. The SCP, as well as its constituent components ESRH and EBWD, discriminated well between the disorganized tornadic storms and the three classes of supercells (discrete, cell in cluster, and cell in line), in agreement with the prior work of T03 and T07. The linear hybrid and QLCS cases populated a part of the EBWD and ESRH parameter spaces similar to the supercells, with lesser vertical shear in the marginal supercell cases. The discrete and cluster RMs occurred in environments of slightly greater MUCAPE, and the linear convective modes displayed MUCAPE approximately 500 J kg^{-1} lower across the distribution. Overall, environmental differences between the supercells and linear modes were relatively small, indicating that point measures of buoyancy and vertical wind shear alone are not able to clearly discriminate between storm modes in a practical sense. Thus, convective mode forecasts must necessarily rely on factors such as shear vector and mean wind orientation to the storm initiation focus [i.e., a surface dryline or cold front, after Dial et al. (2010)], the magnitude of the ascent along the initiating boundary, as well as initial storm spacing and potential storm interactions (Bluestein and Weisman 2000).

The effective-layer STP and its components (MLCAPE, MLLCL height, MLCIN, ESRH, and EBWD) were also examined in seasonal comparisons of sigtor RM and EF1+ tornadic QLCS events. Despite the overall tendency for vertical shear parameters (e.g., EBWD) to discriminate well between tornadic and nontornadic supercells, vertical shear magnitude in the winter provided little insight into the differences between sigtor RM and QLCS tornado events. Despite relatively small values compared to spring and summer, MLCAPE in the winter best differentiated between the QLCS tornadoes and sigtor RM events. During the other seasons, deeper-layer (0–6-km BWD and EBWD) and low-level vertical shear (0–1-km SRH and ESRH) tended to be smaller for QLCS tornadoes compared to sigtor RMs. The combination of ingredients in the effective-layer STP clearly highlighted the sigtor RM environments in the spring, which also represented the most common season for sigtor RMs. While effective-layer STP was not particularly large in the winter, fall, and summer compared to the spring, an approximate STP threshold

around 1 still provided some ability to differentiate between tornadic QLCS and sigtor RM environments.

Storm attributes such as mesocyclone strength and tornado damage ratings both tended to increase in conjunction with composite parameters supporting supercells and tornadoes (e.g., effective-layer SCP and STP). Our findings reinforce a diagnostic recipe that combines storm environment (i.e., large values of effective-layer STP) and convective mode (RM) with mesocyclone strength to favor the production of the more intense (EF3+) tornadoes. Specifically, the more common scenario favoring the production of EF3+ tornadoes includes multiple and/or long-lived supercells with strong mesocyclones, in an environment characterized by the upper end of the STP distribution (i.e., approximately ≥ 4).

The convective mode database will continue to be expanded on a yearly basis. Additional plans include broadening the SPC archive of variables and parameters related to all severe convective events, and not limited to the RM and QLCS tornadoes emphasized in this initial work. Future work with the expanded database will include seasonal environmental characteristics of the sighail and sigwind events by convective mode, as well as temporal changes in convective modes as a function of storm environment. Another goal will be to use the convective mode database as a foundation for multifaceted forecast verification at the SPC.

Acknowledgments. The authors thank Russ Schneider and Steve Weiss of the SPC for their insight and encouragement in the design and development of the convective mode database. The thought-provoking and thorough reviews by Matt Bunkers, Les Lemon, and one anonymous reviewer helpful clarify and strengthen our presentation.

REFERENCES

Andra, D. L., Jr., 1997: The origin and evolution of the WSR-88D mesocyclone recognition nomogram. Preprints, *28th Conf. on Radar Meteor.,* Austin, TX, Amer. Meteor. Soc., 364–365.

Beebe, R. G., 1955: Types of airmasses in which tornadoes occur. *Bull. Amer. Meteor. Soc.,* **36,** 349–350.

——, 1958: Tornado proximity soundings. *Bull. Amer. Meteor. Soc.,* **39,** 195–201.

Benjamin, S. G., and Coauthors, 2004: An hourly assimilation–forecast cycle: The RUC. *Mon. Wea. Rev.,* **132,** 495–518.

Bluestein, H. B., and M. L. Weisman, 2000: The interaction of numerically simulated supercells initiated along lines. *Mon. Wea. Rev.,* **128,** 3128–3149.

Bothwell, P. D., J. A. Hart, and R. L. Thompson, 2002: An integrated three-dimensional objective analysis scheme in use at the Storm Prediction Center. Preprints, *21st Conf. on Severe Local Storms,* San Antonio, TX, Amer. Meteor. Soc., JP3.1. [Available online at https://ams.confex.com/ams/SLS_WAF_NWP/techprogram/paper_47482.htm.]

Brooks, H. E., C. A. Doswell III, and J. Cooper, 1994: On the environments of tornadic and nontornadic mesocyclones. *Wea. Forecasting,* **9,** 606–618.

Bunkers, M. J., B. A. Klimowski, J. W. Zeitler, R. L. Thompson, and M. L. Weisman, 2000: Predicting supercell motion using a new hodograph technique. *Wea. Forecasting,* **15,** 61–79.

Cohen, A. E., 2010: Indices of violent tornado environments. *Electron. J. Oper. Meteor.,* **11,** 2010-EJ6. [Available online at http://www.nwas.org/ej/pdf/2010-EJ6.pdf.]

Craven, J. P., and H. E. Brooks, 2004: Baseline climatology of sounding derived parameters associated with deep moist convection. *Natl. Wea. Dig.,* **28,** 13–24.

Davies, J. M., 2004: Estimations of CIN and LFC associated with tornadic and nontornadic supercells. *Wea. Forecasting,* **19,** 714–726.

——, and A. Fischer, 2009: Environmental characteristics associated with nighttime tornadoes. *Electron. J. Oper. Meteor.,* **10,** 2009-EJ3. [Available online at http://www.nwas.org/ej/pdf/2009-EJ3.pdf.]

Davies-Jones, R. P., D. W. Burgess, and M. Foster, 1990: Test of helicity as a tornado forecast parameter. Preprints, *16th Conf. on Severe Local Storms,* Kananaskis Park, AB, Canada, Amer. Meteor. Soc., 588–592.

Dial, G. L., J. P. Racy, and R. L. Thompson, 2010: Short-term convective mode evolution along synoptic boundaries. *Wea. Forecasting,* **25,** 1430–1446.

Doswell, C. A., III, 1987: The distinction between large-scale and mesoscale contribution to severe convection: A case study example. *Wea. Forecasting,* **2,** 3–16.

——, and E. N. Rasmussen, 1994: The effect of neglecting the virtual temperature correction on CAPE calculations. *Wea. Forecasting,* **9,** 625–629.

——, and D. M. Schultz, 2006: On the use of indices and parameters in forecasting severe storms. *Electron. J. Severe Storms Meteor.,* **1.** [Available online at http://www.ejssm.org/ojs/index.php/ejssm/article/viewArticle/11/12.]

Duda, J. D., and W. A. Gallus Jr., 2010: Spring and summer midwestern severe weather reports in supercells compared to other morphologies. *Wea. Forecasting,* **25,** 190–206.

Edwards, R., A. R. Dean, R. L. Thompson, and B. T. Smith, 2012: Convective modes for significant severe thunderstorms in the contiguous United States. Part III: Tropical cyclone tornadoes. *Wea. Forecasting,* in press.

Fawbush, E. J., and R. C. Miller, 1954: The types of air masses in which North American tornadoes form. *Bull. Amer. Meteor. Soc.,* **35,** 154–165.

Gallus, W. A., Jr., N. A. Snook, and E. V. Johnson, 2008: Spring and summer severe weather reports over the Midwest as a function of convective mode: A preliminary study. *Wea. Forecasting,* **23,** 101–113.

Grams, J. S., R. L. Thompson, D. V. Snively, J. A. Prentice, G. M. Hodges, and L. J. Reames, 2012: A climatology and comparison of parameters for significant tornado events in the United States. *Wea. Forecasting,* **27,** 106–123.

Houston, A. L., R. L. Thompson, and R. Edwards, 2008: The optimal bulk wind differential depth and the utility of the upper-tropospheric storm-relative flow for forecasting supercells. *Wea. Forecasting,* **23,** 825–837.

Johns, R. H., and C. A. Doswell III, 1992: Severe local storms forecasting. *Wea. Forecasting,* **7,** 588–612.

——, J. M. Davies, and P. W. Leftwich, 1993: Some wind and instability parameters associated with strong and violent tornadoes. 2. Variations in the combinations of wind and instability parameters. *The Tornado: Its Structure, Dynamics, Prediction, and Hazards, Geophys. Monogr.,* Vol. 79, Amer. Geophys. Union, 583–590.

Markowski, P., C. Hannon, J. Frame, E. Lancaster, A. Pietrycha, R. Edwards, and R. Thompson, 2003: Characteristics of vertical wind profiles near supercells obtained from the Rapid Update Cycle. *Wea. Forecasting,* **18,** 1262–1272.

McNulty, R. P., 1978: On upper tropospheric kinematics and severe weather occurrence. *Mon. Wea. Rev.,* **106,** 662–672.

——, 1985: A conceptual approach to thunderstorm forecasting. *Natl. Wea. Dig.,* **10** (2), 26–30.

Potvin, C. K., K. L. Elmore, and S. J. Weiss, 2010: Assessing the impacts of proximity sounding criteria on the climatology of significant tornado environments. *Wea. Forecasting,* **25,** 921–930.

Rasmussen, E. N., 2003: Refined supercell and tornado forecast parameters. *Wea. Forecasting,* **18,** 530–535.

——, and D. O. Blanchard, 1998: A baseline climatology of sounding-derived supercell and tornado forecast parameters. *Wea. Forecasting,* **13,** 1148–1164.

Schneider, R. S., and A. R. Dean, 2008: A comprehensive 5-year severe storm environment climatology for the continental United States. Preprints, *24th Conf. Severe Local Storms,* Savannah, GA, Amer. Meteor. Soc., 16A.4. [Available online at http://ams.confex.com/ams/pdfpapers/141748.pdf.]

Schoen, J. M., and W. S. Ashley, 2011: A climatology of fatal convective wind events by storm type. *Wea. Forecasting,* **26,** 109–121.

Shafer, C. M., A. E. Mercer, L. M. Leslie, M. B. Richman, and C. A. Doswell III, 2010: Evaluation of WRF model simulations of tornadic and nontornadic outbreaks occurring in the spring and fall. *Mon. Wea. Rev.,* **138,** 4098–4119.

Showalter, A. K., and J. R. Fulks, 1943: Preliminary report on tornadoes. U.S. Weather Bureau, 162 pp.

Smith, B. T., R. L. Thompson, J. S. Grams, C. Broyles, and H. E. Brooks, 2012: Convective modes for significant severe thunderstorms in the contiguous United States. Part I: Storm classification and climatology. *Wea. Forecasting,* **27,** 1114–1135.

Stumpf, G. J., A. Witt, E. D. Mitchell, P. L. Spencer, J. T. Johnson, M. D. Eilts, K. W. Thomas, and D. W. Burgess, 1998: The National Severe Storms Laboratory mesocyclone detection algorithm for the WSR-88D. *Wea. Forecasting,* **13,** 304–326.

Thompson, R. L., R. Edwards, J. A. Hart, K. L. Elmore, and P. Markowski, 2003: Close proximity soundings within supercell environments obtained from the Rapid Update Cycle. *Wea. Forecasting,* **18,** 1243–1261.

——, ——, and C. M. Mead, 2004: An update to the supercell composite and significant tornado parameters. Preprints, *22nd Conf. Severe Local Storms,* Hyannis, MA, Amer. Meteor. Soc., P8.1. [Available online at https://ams.confex.com/ams/11aram22sls/techprogram/paper_82100.htm.]

——, C. M. Mead, and R. Edwards, 2007: Effective storm-relative helicity and bulk shear in supercell thunderstorm environments. *Wea. Forecasting,* **22,** 102–115.

Trapp, R. J., S. A. Tessendorf, E. S. Godfrey, and H. E. Brooks, 2005: Tornadoes from squall lines and bow echoes: Part I: Climatological distribution. *Wea. Forecasting,* **20,** 23–34.

Weisman, M. L., and J. B. Klemp, 1982: The dependence of numerically simulated convective storms on vertical wind shear and buoyancy. *Mon. Wea. Rev.,* **110,** 504–520.

Wilks, D. S., 1995: *Statistical Methods in the Atmospheric Sciences: An Introduction.* Academic Press, 467 pp.